

UC Davis

Recent Work

Title

High temperature elemental losses and mineralogical

Permalink

<https://escholarship.org/uc/item/0w92z6bs>

Authors

Thy, P.

Jenkins, B. M.

Grundvig, S.

et al.

Publication Date

2006

Peer reviewed

High temperature elemental losses and mineralogical changes in common biomass ashes

P. Thy^{a,*}, B.M. Jenkins^b, S. Grundvig^c, R. Shiraki^d, C.E. Lesher^a

^a Department of Geology, University of California, One Shields Avenue, Davis, CA 95616, USA

^b Department of Biological and Agricultural Engineering, University of California, One Shields Avenue, Davis, CA 95616, USA

^c Department of Earth Sciences, Aarhus University, DK-8000 Århus C, Denmark

^d Interdisciplinary Center for Plasma Mass Spectrometry and McClellan Nuclear Radiation Center, University of California, Davis, CA 95616, USA

Received 22 December 2004; received in revised form 16 August 2005; accepted 16 August 2005

Available online 15 September 2005

Abstract

The elemental losses from ashes of common biomass fuels (rice straw, wheat straw, and wood) were determined as a function of temperature from 525 °C to below 1525 °C, within the respective melting intervals. The experimental procedure was chosen to approach equilibrium conditions in an oxidizing atmosphere for the specific ash and temperature conditions. All experiments were conducted in air and used the ashes produced initially at temperatures of 525 °C as reactants. Losses during the initial ashing at 525 °C were negligible, except for a K₂O loss of 26% for wood and a Cl loss of 20% for wheat straw. Potassium losses are positively correlated with temperature for all fuel ashes. The K₂O loss for wood ash commences at 900–1000 °C. Carbonate is detected in the wood ashes to about 700–800 °C and thus cannot explain the retention of K₂O in the ashes to 1000 °C. Other crystalline phases detected in the wood ashes (periclase and larnite) contain little or no potassium. Petrographic examinations of high temperature, wood ash products have failed to reveal potassium bearing carbonates, sulfates, or silicates. The release of potassium, thus, appears to be unrelated to the breakdown of potassium-bearing crystalline phases. The straw ashes show restricted potassium loss compared to wood ash. The potassium content declines for both straw ashes from about 750 °C. Cristobalite appears in the straw ashes at about 700–750 °C and is replaced by tridymite in the rice straw ash from about 1100 °C. Sylvite (KCl) disappears completely above 1000 °C. The Cl content starts to decline at about 700 °C, approximately at the same temperature as potassium, suggesting that the breakdown of sylvite is responsible for the losses. The K–Cl relations demonstrate that about 50% of K (atomic basis) released from breakdown of sylvite is retained in the ash. The presence of chlorine in the ash is, therefore, best attributed to the presence of sylvite. Potassium is easily accommodated in the silicate melt formed at temperatures perhaps as low as 700–800 °C from dehydration, recrystallization, and partial melting of amorphous components. Loss of potassium persists for ashes without remaining sylvite and points to the importance of release of potassium from partial melt at temperatures within the melting interval for the fuel ashes.

© 2005 Elsevier Ltd. All rights reserved.

Keywords: Biomass; Wood; Rice straw; Wheat straw; Ash; Slag; High temperature; Mineral transformations; Alkali metal losses

1. Introduction

Knowledge of the retention or volatilization of alkali metal and halogen elements in ash during combustion of biomass fuels is important for an efficient and economically viable large-scale utilization of many field crop residues and future energy crops. Combustion in biomass fueled boilers, using stoker-fired grate furnaces, fluidized beds, and suspension units, can lead to a rapid build-up of unmanageable deposits on

fireside surfaces, especially superheaters. Such deposits retard the rate of heat transfer, reduce efficiency, and increase corrosion of metal surfaces. More advanced technologies that offer substantial increase in thermal efficiency, such as biomass integrated gasifier combined cycles, may in some cases prove even more sensitive to fouling.

Annual growth plant materials, including straws and grasses, contain high concentrations of alkali and alkaline earth metals, silicon, and chlorine [1–3]. Potassium is the alkali metal present in largest concentration and its volatilization during firing is directly linked to formation of tenacious surface deposits. Chloride is an important facilitator for the deposition of alkali components. At flame temperature, potassium is deposited as KCl or KOH dependent on the availability of chlorine. At lower temperatures, KCl may react with sulfur or

* Corresponding author. Tel.: +1 530 752 0359; fax: +1 530 752 0951.

E-mail address: thy@geology.ucdavis.edu (P. Thy).

carbon components of the gas to produce either sulfates or carbonates that readily precipitate on boiler surfaces. Sulfur can also react with potassium in surface deposits to form sulfates [3–6]. It is commonly, perhaps intuitively, assumed that chlorine is easily evaporated and acts as a high temperature transport media for potassium [3,7]. This appears to be supported by the presence of sylvite crystals in some boiler deposits [8]. Controlled and simplified laboratory experiments have shown that volatilization of potassium, within slag melting temperatures, is strongly controlled by the fuel composition and that potassium is retained in molten rice straw ash, but evaporated from molten wood ash [9]. Use of a straw component in fuel blends was predicted to restrict fouling [10]. These findings require a systematic study of the elemental losses during combustion and ash and slag formation. The halogen elements have been suggested to play an important role in the elemental flux in combustion systems, but such effects have not been investigated in controlled and simplified laboratory experiments [9–11].

We present here the result of a pilot study of the compositional and mineralogical effects on ash and slag by burning fuel at temperatures from within the ashing range to near complete melting. In particular, we evaluate the co-variation of potassium and chlorine concentrations for three commonly available biomass fuels in California (wood, rice straw, wheat straw). Of these three, currently only wood is used

as fuel in California due to problems such as fouling, slugging, and in fluidized beds also agglomeration of the bed medium observed with straw in operating power boilers. Straw is used in boilers elsewhere, especially Europe, where designs have been adopted that better allow the ash to cool below the liquidus prior to encountering cross-flow heat transfer surfaces. Although heating rates and furnace gas compositions in operating boilers were not entirely matched in this study, results are relevant to the formation of slag and agglomerates often found under oxidizing conditions.

2. Fuel selection and ash preparation

The samples selected for the ashing experiments are three commonly available biomass materials in California. The first is a mixed conifer (white fir and ponderosa pine) whole-tree chip fuel obtained from Wheelabrator-Shasta Energy Company, Inc., Anderson, California. The trees were harvested from the northeastern slopes of Mt. Shasta. This relatively clean and high quality fuel is one of many types received at the plant. The second sample is a medium grain Japonica (variety M202) rice straw from Colusa County, California. The third sample is a wheat straw from Yolo County, California. Neither of the straw fuels is currently used as boiler fuel in California, although several facilities are permitted to use straw.

Table 1
Compositions of fuels used as starting materials

	Wood		Rice straw		Wheat straw	
Ultimate analysis (% wet basis)						
Carbon	48.54		38.50		43.81	
Hydrogen	5.22		3.56		5.10	
Nitrogen	0.07		0.55		0.58	
Sulfur	0.02		0.06		0.12	
Oxygen	34.66		29.23		33.50	
Moisture	10.4		7.5		7.8	
Chlorine	<0.012		0.648		0.402	
Potassium	0.075		0.996		0.593	
Ash (% dry basis)	1.2		22.1		9.8	
	Wood	Volatile free	Rice straw	Volatile free	Wheat straw	Volatile free
Ash analysis (% oxides)						
SiO ₂	9.35	14.01	75.38	82.13	57.47	70.28
TiO ₂	0.13	0.19	0.01	0.01	0.05	0.06
Al ₂ O ₃	3.12	4.68	0.09	0.10	0.77	0.94
Fe ₂ O ₃	1.14	1.71	0.10	0.11	0.39	0.48
MnO	1.76	2.64	0.27	0.29	0.07	0.09
MgO	4.93	7.39	1.64	1.79	1.82	2.23
CaO	32.06	48.05	1.60	1.74	2.8	3.42
Na ₂ O	0.39	0.58	0.14	0.15	0.8	0.98
K ₂ O	10.72	16.06	11.95	13.02	16.55	20.24
P ₂ O ₅	3.13	4.69	0.61	0.66	1.05	1.28
L.O.I.	27.59		7.97		14.91	
Total	94.32	100.00	99.76	100.00	96.68	100.00
SO ₂	0.69		0.67		1.66	
Cl	<0.065		3.18		3.58	
CO ₂	6.24		0.22		0.19	

Ultimate analyses by Hazen Research, Inc., Golden, CO, except that Cl and K determined at UCD by INAA. Ashing temperature was 525 °C. Ash composition determined at University of Aarhus, except SO₂ and CO₂ determined by Hazen and Cl determined at UCD by INAA. L.O.I. is the loss-on-ignition determined from heating the ash to 950 °C.

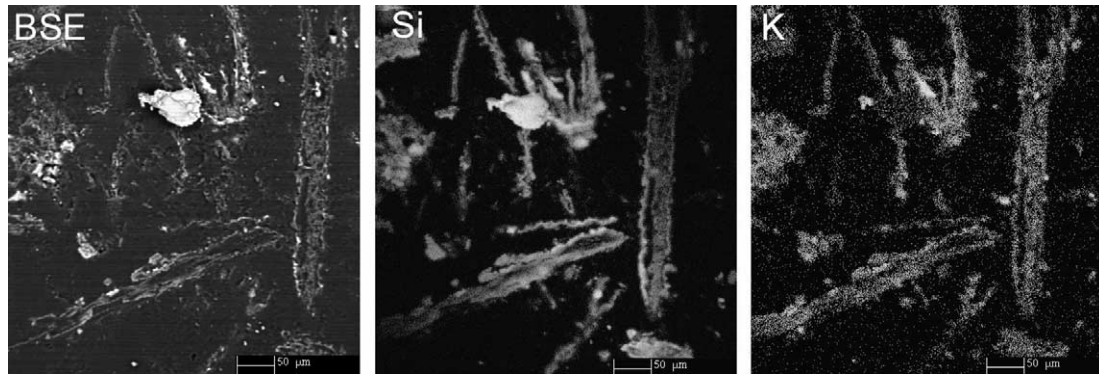


Fig. 1. Back-scattered electron image (BSE) and elemental X-ray dot-maps of K_{α} lines for Si and K of rice straw ash. Two different types of particles are present: elongated highly porous particles of biogenic origin and irregular silicic particles of likely terrigenous origin. The irregular mottling of the matrix is due to surface temperature damages to the epoxy. The scale bars are 50 μm .

The fuels were dried in ambient air for a week and then milled to a maximum 1/8" (3 mm) particle size. The final moisture content for the samples determined after oven-drying at 105 °C were, on a wet basis, 10.4% for wood, 7.5% for rice straw, and 7.8% for wheat straw.

The fuels were ashed in air in a large-volume, electric muffle furnace. Temperature was ramped at 20 °C/min to 100 °C and then at 2 °C/min to a maximum of 525 °C. Temperature was dwelled at 400 °C for 3 h and again at 525 °C for 4 h. The furnace temperature was then dropped from the maximum 525 °C by 8 °C/min until 30 °C. The furnace and sample temperatures were monitored during ashing by thermocouples inserted through the roof of the furnace. The rice and wheat straw samples were ashed in open ceramic containers. The wood sample was ashed in a semi-closed, steel container with an airflow of 4.5 L/min admitted to the container when temperature reached its maximum value. These ashing procedures allowed relatively large ash volumes to be produced under controlled temperatures without ignition. Such ignition could have resulted in uncontrolled high temperature and possible elemental losses. The ash samples were stored in airtight containers before and between uses.

The total amounts of dried fuel used were 22.2 kg wood giving an ash content on a dry basis of 1.2%, 2.3 kg of rice straw giving an ash content 22.1%, and 4.5 kg wheat straw giving an ash content of 9.8% (all for ashing at 525 °C). The ultimate elemental compositions for the fuels were determined following the analytical recommendations of Miles et al. [6]. The major and minor oxide compositions of the ash fractions were determined by X-ray fluorescence and the potassium and chlorine contents were determined by instrumental neutron activation (Section 5). The compositions of the fuel samples are summarized in Table 1.

3. Ash characterization

To further characterize the ashes, various light and electron microscopic techniques were used. Scanning electron microscope images (back-scattered electron (BSE) images and elemental X-ray dot-maps) show that the straw ash particles have typical elongated shapes reflecting biogenic origins

(Fig. 1). Rice and wheat straw ashes are morphologically and compositionally very similar (Figs. 1 and 2). The particles typically measure up to 1 mm long and 50 μm wide and are highly porous with an inner intricate network of walls. The elemental distributions of Si and K are irregular with outer walls often containing higher concentrations of Si. The biogenic wheat straw ash particles have rims with high concentrations of potassium seen as a high mean-atomic density in BSE images (Fig. 2). Irregular shaped high-Si particles, containing minor, but variable amounts of Ca, Al, and Mg are also present and are of terrigenous origin (soil particles). The X-ray diffraction pattern reveals that in addition sylvine (KCl) is present and that the main part of the ash particles are composed of non-crystalline, amorphous compounds (Fig. 3). Sylvite is frequently observed after ashing or burning of rice straw and other grasses [8].

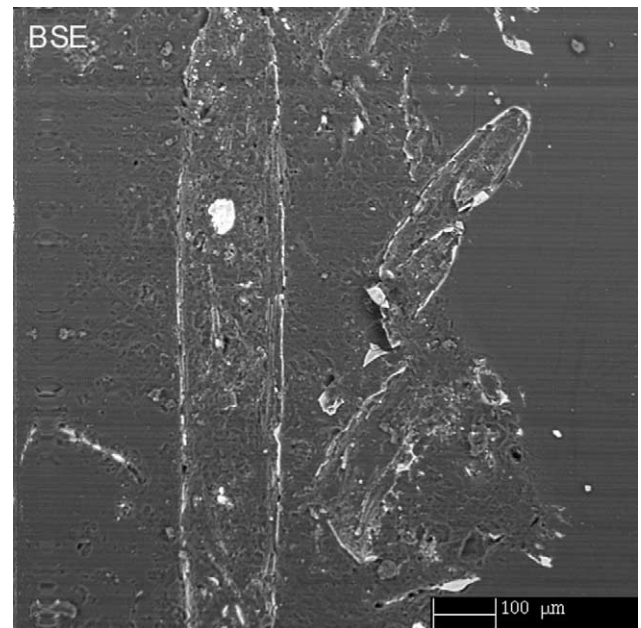


Fig. 2. Back-scattered electron image (BSE) of wheat straw ash. The irregular mottling of the matrix is due to surface temperature damages to the epoxy. The scale bars are 100 μm .

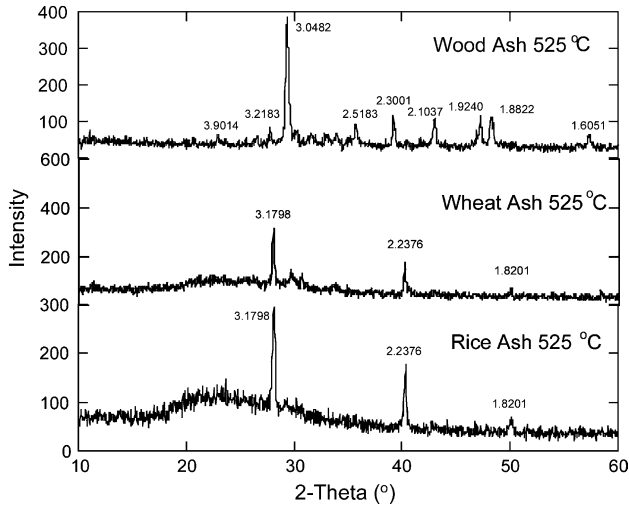


Fig. 3. XRD patterns (Cu K_{α} radiation) for the ashes produced at 525 °C. Measured d -values are in ångstrom. Wood ash shows diffraction pattern for calcite. The rice and wheat straw ashes show the diffraction pattern for sylvine (KCl) and amorphous silica (broad background between 20 and 30° 2θ). Intensity is counts per second. 2θ is the angle 2θ in degrees.

The wood ash is very fine-grained and rarely contains particles above 20 μm in length or diameter. Individual groups of particles range in shape from fibrous to round (Fig. 4). The general shapes of the grains can be related to their compositions. Needle shaped particles are Si-rich, angular particles are Ca-rich (likely carbonates), and irregular to

rounded particles are Si- and K-rich. The X-ray diffraction pattern shows that the only crystalline material detectable is calcite (Fig. 3). The needle-shaped grains are composed of amorphous silica.

4. Experimental techniques

For each experiment, about 20 g of ash powder was pressed into a pellet at pressures up to 3000 psi (21 MPa). The pellets were placed in a bottom-fed, Kanthal furnace at a temperature between the original ashing temperature of 525 °C and their respective melting temperatures in intervals of about 50 °C for straws and 100 °C for wood. The pellets were raised into the hot zone of the furnace and kept there for 2 h for straw ashes or 3 h for wood ash. The furnace and sample temperatures were monitored by an S-type thermocouple placed near the pellet and inserted through the top of the furnace. Typically, the sample heated to the maximum at 20 °C/min. Lowering the furnace bottom cooled the pellet to ambient temperature and terminated the experiment. Pellets were placed on Pt foil to avoid reaction with the alumina bottom plate. The experimental products were powdered in an agate mortar or if required using a SPEX wolfram carbide mill for about 2 min. The color of the powder was measured by using a BYK-Gardner Colour Guide 6805 (L^* lightness; a^* red/green, b^* yellow/blue). The experimental temperatures are together with the results summarized in Table 2.

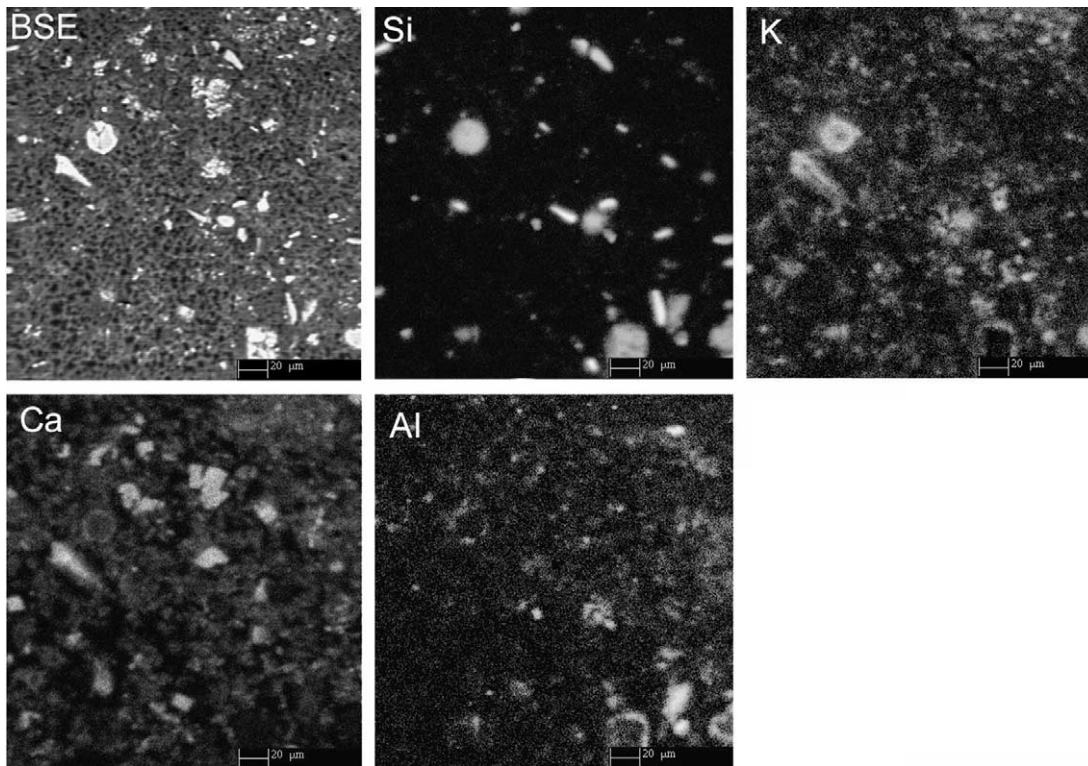


Fig. 4. Back-scattered electron image (BSE) and elemental X-ray dot maps of K_{α} lines for Si, K, Ca, and Al of wood ash. Three fundamental types of particles are present: elongated Si-rich particles, angular Ca-rich particles, and rounded Si- and K-rich particles. The maximum grain size is below 20 μm . The irregular mottling of the matrix is due to surface temperature damages to the epoxy. The scale bars are 20 μm .

Table 2
XRF analyses of ash (wt% oxides)

ID	T (°C)	Loss (%)	SiO ₂	TiO ₂	Al ₂ O ₃	Fe ₂ O ₃	MnO	MgO	CaO	Na ₂ O	K ₂ O	P ₂ O ₅	L.O.I. (950 °C)	Cl (INA)	Sum	Sum (-O=Cl)	K ₂ O (INA)	Ash color		
																		L*	a*	b*
Wood																				
WO-8	1525		12.76	0.15	6.87	1.48	2.27	7.35	45.55	0.35	6.96	4.38	9.33		97.44			52.28	-2.80	4.28
WO-10	1425	36.2	13.42	0.16	4.54	1.63	2.55	7.68	48.84	0.40	6.59	4.87	6.39	<0.067	97.08		7.53	45.93	3.36	11.25
WO-7	1325	32.6	13.23	0.16	4.36	1.56	2.45	7.35	46.82	0.46	7.40	4.68	8.24		96.70			47.94	1.48	8.57
WO-9	1225		12.00	0.16	4.13	1.47	2.36	6.87	44.40	0.49	11.44	4.42	8.74		96.46			51.02	0.44	8.17
WO-6	1125	27.5	12.06	0.15	3.90	1.39	2.22	6.44	41.27	0.50	12.78	4.11	11.42	<0.067	96.24		11.74	46.51	0.50	7.23
WO-1	1011	27.3	12.35	0.15	3.66	1.37	2.08	6.05	39.25	0.49	12.97	3.92	13.67		95.97			49.65	1.36	10.34
WO-5	913	25.2	11.69	0.15	3.79	1.35	2.10	6.07	39.47	0.50	13.70	3.92	13.33		96.08			49.30	0.20	9.13
WO-4	816	21.9	11.72	0.13	3.71	1.32	2.09	6.03	39.03	0.49	13.34	3.85	13.94	<0.104	95.66		13.62	45.83	2.29	6.60
WO-3	718	9.9	10.14	0.12	3.25	1.19	1.87	5.33	34.50	0.43	11.74	3.38	22.94		94.89			53.10	1.04	5.02
WO-2	621	4.2	9.46	0.12	3.06	1.12	1.77	5.04	32.49	0.39	10.89	3.18	26.73		94.26			57.82	0.84	7.86
WO-S	524		9.35	0.13	3.12	1.14	1.76	4.93	32.06	0.39	10.72	3.13	27.59	<0.065	94.31		12.29	62.45	1.23	11.63
WO-raw														<0.012			0.180			
Wheat straw																				
WH-5	962	18.5	66.91	0.06	0.94	0.46	0.07	2.15	3.17	0.98	17.71	1.18	4.75	2.80	101.18	99.91	18.79	69.01	1.66	10.02
WH-4	913	16.3	66.35	0.05	0.89	0.42	0.07	2.12	3.12	0.91	18.00	1.16	5.27	3.32	101.70	100.20	19.91	66.36	1.45	9.39
WH-6	864	15.5	66.76	0.06	0.97	0.48	0.07	2.09	3.11	0.93	18.05	1.13	5.25	3.69	102.57	100.91	19.71	63.42	0.78	7.91
WH-3	816	14.5	65.45	0.05	0.91	0.44	0.08	2.10	3.12	0.92	18.85	1.17	4.92	3.86	101.88	100.14	20.49	61.26	0.34	5.35
WH-7	767	13.8	66.20	0.05	0.90	0.44	0.07	2.05	3.10	0.90	18.53	1.12	3.51	4.12	100.99	99.13	20.16	57.12	0.07	2.82
WH-2	718	13.9	64.72	0.05	0.80	0.39	0.07	2.06	3.06	0.89	19.32	1.14	3.32	4.27	100.10	98.17	20.09	54.25	0.57	2.12
WH-8	670	12.5	65.23	0.06	0.92	0.44	0.07	2.03	3.00	0.89	18.38	1.08	4.17	4.24	100.51	98.60	19.34	50.64	0.67	1.74
WH-1	621	12.1	62.88	0.05	0.77	0.34	0.07	1.98	2.97	0.87	18.57	1.10	6.94	4.12	100.65	98.79	19.37	52.74	0.27	-0.24
WH-9	572	10.5	63.69	0.06	0.94	0.43	0.07	1.94	2.88	0.85	17.36	1.02	7.26	3.99	100.50	98.70	18.65	54.95	0.37	-0.09
WH-S	524		57.47	0.05	0.77	0.39	0.07	1.82	2.80	0.80	16.55	1.05	14.91	3.58	100.27	98.65	17.41	50.79	-0.09	0.00
WH-raw														0.402			1.43			
Rice straw																				
R-13	1325		83.12	0.03	0.13	0.09	0.39	2.01	2.34	0.16	10.06	0.49	0.59	0.35	99.74	99.66	9.90	49.83	0.23	1.25
R-12	1225	14.6	79.94	0.02	0.12	0.09	0.39	2.00	2.34	0.17	10.16	0.64	0.28	<0.023%	96.13	96.13	9.69	85.34	2.76	0.21
R-11	1125	14.0	82.94	0.03	0.14	0.09	0.39	2.02	2.34	0.17	10.13	0.68	0.71	<0.026%	99.65	99.65	10.39	84.56	3.54	-0.79
R-10	1011	10.6	79.90	0.01	0.12	0.12	0.37	1.93	2.21	0.21	11.35	0.67	2.85	1.71	101.46	101.07	12.13	82.02	3.21	-0.44
R-5	962	9.6	78.84	0.02	0.13	0.11	0.36	1.90	2.15	0.21	11.81	0.65	3.98	2.27	102.45	101.93	12.50	82.15	2.55	1.37
R-4	913	8.7	77.77	0.01	0.12	0.10	0.36	1.88	2.14	0.21	12.19	0.65	4.65	2.81	102.89	102.25	13.01	80.34	2.37	2.03
R-6	864	8.1	77.59	0.01	0.12	0.10	0.35	1.86	2.11	0.19	12.37	0.65	4.82	2.89	103.07	102.42	12.68	79.60	1.80	2.67
R-3	816	7.7	76.90	0.02	0.11	0.09	0.35	1.84	2.11	0.19	12.48	0.64	5.35	3.17	103.25	102.53	14.14	74.42	1.21	2.11
R-7	767	7.3	76.54	0.01	0.12	0.09	0.35	1.85	2.11	0.19	12.60	0.64	5.85	3.20	103.54	102.82	13.48	65.85	1.03	1.66
R-2	718	7.0	76.04	0.01	0.12	0.09	0.35	1.84	2.10	0.18	12.47	0.63	6.59	3.39	103.82	103.05	13.80	62.74	1.14	0.16
R-8	670	6.1	75.33	0.01	0.11	0.09	0.34	1.82	2.06	0.18	12.54	0.63	7.18	3.25	103.54	102.81	13.06	60.06	0.64	-0.05
R-1	621	5.7	75.16	0.01	0.11	0.08	0.34	1.81	2.05	0.18	12.49	0.63	7.18	3.45	103.51	102.73	13.41	57.68	0.30	0.10
R-9	572	5.5	74.47	0.01	0.11	0.09	0.35	1.82	2.05	0.18	12.28	0.62	7.95	3.21	103.15	102.43	12.69	53.59	0.76	0.09
R-S	524		72.55	0.01	0.11	0.08	0.34	1.74	2.00	0.16	11.33	0.60	10.94	3.18	103.05	102.33	12.47	48.16	0.08	-0.26
R-raw														0.638			2.40			

(continued on next page)

Table 2 (continued)

ID	T (°C)	Loss (%)	SiO ₂	TiO ₂	Al ₂ O ₃	Fe ₂ O ₃	MnO	MgO	CaO	Na ₂ O	K ₂ O	P ₂ O ₅	L.O.I. (950 °C)	Cl (INA)	Sum	Sum (-O=Cl)	K ₂ O (INA)	Ash color	
																		L*	a*
NB-S1633a			48.61	1.37	27.07	13.65	0.02	0.79	1.54	0.21	2.24	0.39	3.19			99.08			
Rec-ommen-			48.78	1.33	27.02	13.44	0.02	0.75	1.55	0.23	2.26	0.38							
ded			0.09	0.01	0.07	0.05	0.01	0.08	0.18	0.03	0.05	0.04							
Uncertainty																			
Wood			0.23	0.01	0.03	0.03	0.01	0.04	0.05	0.04	0.07	0.02		0.06			0.16		
ash																			
Straw																			
ash																			

Analyses referred to as 'raw' is the results of neutron activation analyses on the original raw fuel. L.O.I. (950 °C) is the loss-on-ignition at 950 °C. Cl (INA) is chlorine as determined by neutron activation analyses. K₂O* is the K₂O content determined by neutron activation analyses. Sum (-O=Cl) is the total corrected for oxygen equivalent of chlorine. NBS1633a flyash as analysed and recommended value. Uncertainty is based on counting statistics.

5. Analytical techniques

5.1. X-ray fluorescence

Loss on ignition was determined by heating the powder in air in a muffle furnace at 950 °C for 3 h. Fused glasses were prepared by mixing an amount of unheated powder equivalent to 0.75 g ignited sample with 3.75 g of Fluore-X65 HP (a commercial flux from Socachim Fine Chemicals consisting of 66 wt% Li₂B₄O₇ and 34 wt% LiBO₂) in a 30 ml 95Pt-5Au crucible. The crucible was transferred to a muffle furnace and the contents melted twice for 5 min at 1150 °C with swirling of the crucible between melting. After fusion, the melt was poured into a red-hot, 32 mm 95Pt-5Au mould and quenched with air to produce a flat glass disc.

The XRF major element analyses were performed on a PANalytical PW2400 X-ray spectrometer using SuperQ software. A 3 kW Rh-tube was used operating at 50 kV and 55 mA along with PX-1 multilayer for Na and Mg, PE crystal for Al and Si, Ge crystal for P, LiF(200) crystal for K, Ca and Ti and LiF(220) crystal for Mn and Fe. The detector was a gas flow proportional counter using P10 (10% methane in Ar) gas. For Mn and Fe, this detector was used in tandem with a sealed Xe detector.

A total of 44 international silicate rock reference materials, with compositions ranging from basaltic to rhyolitic, were used for the calibrations [12,13]. Fly ash NBS/NIST 1633a was prepared and analyzed in the same way as the ashes. The results are given in Table 2 together with the recommended values from Govindaraju [12]. Typical uncertainties for wood and straws are also given in Table 2.

5.2. Instrumental neutron activation

About 20–120 mg of powder was heat-sealed in a 0.35 mL polyethylene vial. Five vials, including standard (reagent grade KCl), reference material for quality assurance (NIST Standard Reference Material 1589, non-fat milk powder), and unknown samples, were placed at the bottom of a larger polyethylene tube (17 mm I.D., 11 cm long) to ensure a negligible vertical gradient in neutron flux. The tubes were irradiated in a TRIGA-type nuclear reactor of University of California, Davis, at 1.8 MW power (thermal neutron flux: $\sim 1 \times 10^{13}$ n cm⁻² s⁻¹) for 10 or 30 s using a pneumatic transfer system.

Assay of delayed gamma ray was performed using a Genie-VMS spectroscopy system from Canberra Industries Inc. (Meriden, CT). Detectors of the system were co-axial, high-purity germanium detectors, whose energy resolution was 1.8~2.2 keV for ⁶⁰Co peak at 1332 keV. For each sample, 5 min counting was performed for ³⁸Cl (half-life: 37.2 min) peak at 1643 keV during a decay period of 12–138 min, which was followed by another 10–45 min counting for ⁴²K (half-life: 12.4 h) peak at 1525 keV during a decay period of 51 min to 11.2 h. Precision of analysis was better than 1.2 and 0.2% for K and Cl, respectively. The accuracy estimated from the results of the reference material was better than 3.7 and 6.0% for K and Cl, respectively.

5.3. X-ray diffraction

The X-ray diffraction patterns were determined with an INEL XRG 3000 powder diffractometer, equipped with a CPS 120 detector. Operating conditions were 30 kV and 30 mA. Cu K_{α} radiation was used and the pattern of each sample was acquired with a total collection time of 1000 s. Peak identification was done with the JADE software package (MDI, Livermore, CA) and PDF diffraction database (ICDD, Swarthmore, PA).

6. Results

The results for the biomass ashes are summarized in Table 2, giving the experimental temperatures, weight losses, composition of the ashes, and product color. The major and minor elements of the ashes are given as wt% oxides. The chlorine content is given as elemental wt%. The presence of chlorine requires the oxide totals to be corrected for the oxygen equivalent of chlorine (see footnote to Table 2). In addition to the ashes, the raw fuels were also analyzed for K_2O and Cl using INA techniques.

6.1. Wood ash

The wood ash was fired at temperatures from 621 to 1425 °C without detectable melting. The experimental products are grayish brown to brown and largely unconsolidated. An unidentified bluish-green pigmentation on the surface is sometimes associated with vesicle channels and thus presumably the release of metal compounds (Fe, Mn, Cu, Zn) together with volatiles from the interior of the pellets. The ash color becomes systematically darker until about 800 °C, after which the color is relatively unchanged (L*, Table 2).

The change in weight loss (Fig. 5) can be correlated with mineralogical changes (Fig. 6). Calcite is present to 718 °C, easily identified by the 3.017 Å diffraction peak at $2\theta = 29.4^\circ$. Larnite can be identified in products from 718 °C by a group of three diffraction peaks between 2θ of 34.4 and 31.8° probably

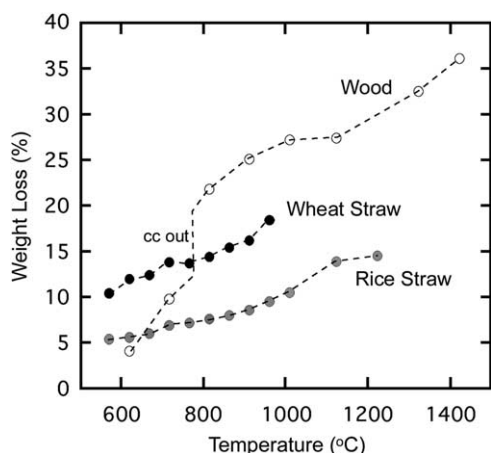


Fig. 5. Weight loss (%) as a function of firing temperature (°C). Disappearance of calcite in the wood ash is indicated (cc-out).

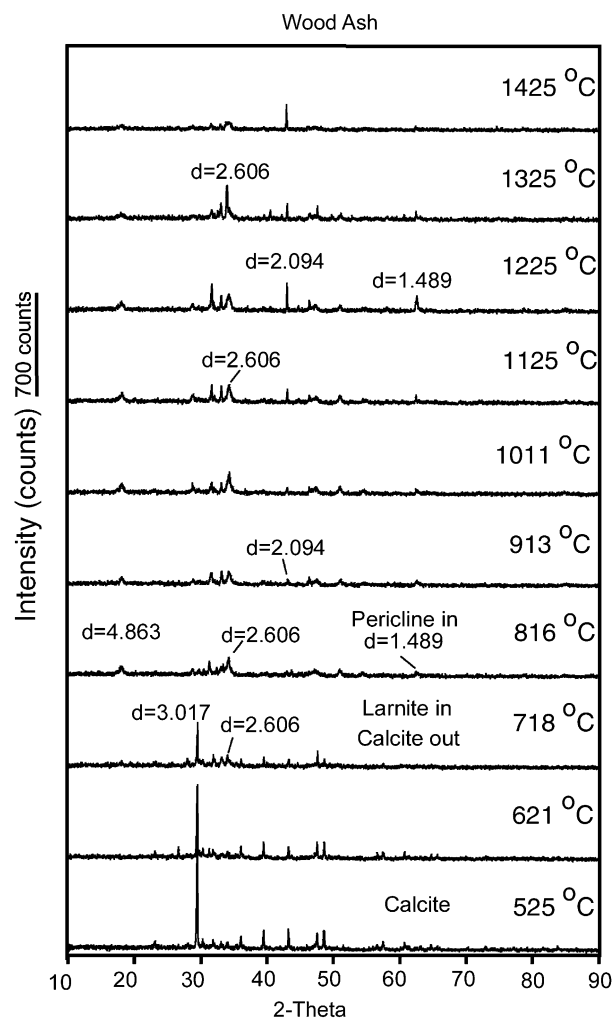


Fig. 6. Summary of XRD patterns (Cu K_{α} radiation) for the wood ashes. Characteristic measured d -values in Å used to identify specific minerals.

representing a larnitic phase ($d = 2.606, 2.696, \text{ and } 2.811$). Pericline can be identified in products from 816 °C by the 2.094 Å ($2\theta = 42.9^\circ$) and the 1.489 Å ($2\theta = 62.3^\circ$) diffraction peaks. The intensities of the larnite peaks increase with increasing temperature until 1425 °C, reflecting increased recrystallized volume, while pericline peaks at 1225 °C. The main change in color and weight loss thus may be due to the breakdown of calcite and the appearance of larnite and pericline in the temperature range of 700–800 °C.

These results to 1425 °C can be compared with high temperature melting experiments conducted on the same wood ash [10]. These experiments estimated a solidus temperature between 1350 and 1390 °C and a liquidus above 2000 °C. A phosphor-containing larnite mineral and pericline coexisting with quenched melt was found in these melting experiments between 1405 and 1540 °C. Additional phases were not detected at or below the solidus. The present results suggest that the appearances of larnite and pericline commence at temperatures within the subsolidus range and only suggest minor amounts of melting to temperatures as high as 1400 °C.

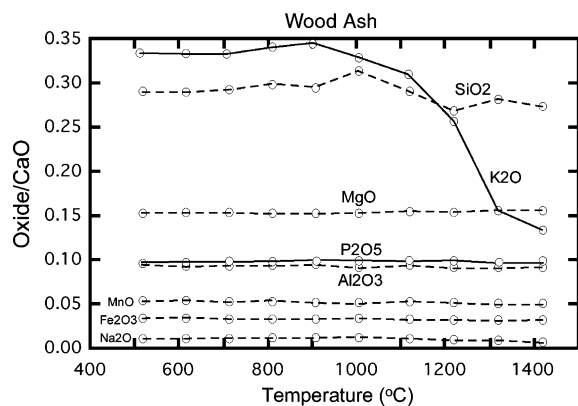


Fig. 7. Composition of the ash fractions expressed as wt% oxides normalized to CaO content and plotted as a function of temperature.

Modeling using the FactSage thermochemical database [14] confirms the high liquidus temperatures of 1900–2000 °C. Calcite breaks down over a wide temperature range from 500 °C and are completely eliminated at 1100 °C due to the stabilization of Na–K carbonates at high temperature. Monoxide minerals (periclase or lime) are variably stable onto the liquidus. The modeling, however, fails to predict the formation of phosphor-bearing larnite that is seen in the experiments [10] and also suggests that release of potassium is restricted to temperatures near or above the liquidus in contrast to the low temperature release observed in the present experiments.

The analytical results are summarized in Fig. 7 as oxides normalized to the CaO concentration (all wt%). This graphical representation of the experimental results assumes that CaO remains unchanged throughout the investigated temperature interval (cf. [9]). The main compositional variation is a marked decrease in K₂O initiated at about 900 °C. The SiO₂ shows a decrease between 1000 and 1200 °C and MgO may show a slight increase from 1000 °C. The remaining major and minor oxides (TiO₂, Na₂O, MnO, Al₂O₃, P₂O₅) show small or no variations. It is unclear whether the variation in SiO₂ and MgO are real or perhaps due to a breakdown in the assumption that CaO is constant. A study of an urban wood ash above its liquidus temperature at 1300 °C [9], however, suggests that CaO concentration is independent of duration at superliquidus conditions. Chlorine was not detected in the wood ash (Table 2).

The weight losses during ashing increases with temperature from 4% to about 36% (Fig. 5). The loss-on-ignition determined at 950 °C (Table 2) vary inversely with the weight loss from ashing. If the two loss determinations are added, the results for ashing above 950 °C are fairly similar to the weight loss measured for the high-temperature melting experiments of Thy et al. [10] (39–42%). This suggests that complete equilibration was not reached during the ashing experiments and that a carbonate compound may have been preserved in the experimental high temperatures products. Likewise, the losses of potassium during the ashing experiments were markedly lower than for the melting experiments where all potassium was lost.

6.2. Rice straw ash

The rice straw ash was fired at temperatures from 572 to 1325 °C well into its melting interval. Significant hardening and sintering of the pellets occurs from the starting temperature of 572 °C. Large-scale melting is apparent at 1325 °C with abundant bubble formation and pellet expansion. The ash color become systematically lighter with increasing temperature and changes from gray to whitish gray at 816 °C and finally pinkish white at 975 °C (L*, Table 2). Colors ranging from violet to pink have been previously observed with rice straw and rice hull ash and are thought to be largely associated with potassium concentration [25]. Ash from rice straw that has first been water-leached to extract potassium and chlorine uniformly exhibits a bright white color.

The mineralogical changes as a function of temperature are summarized in Fig. 8. Sylvite is conspicuously present until 1125 °C and can easily be identified by the 3.146 Å ($2\theta=28.3^\circ$) and the 2.225 Å ($2\theta=40.5^\circ$) diffraction peaks. Cristobalite appears at 767 °C identified by the 4.040 Å diffraction peak ($2\theta=22.0^\circ$). Tridymite appears to replace cristobalite from above 1125 °C. The transformation of cristobalite into

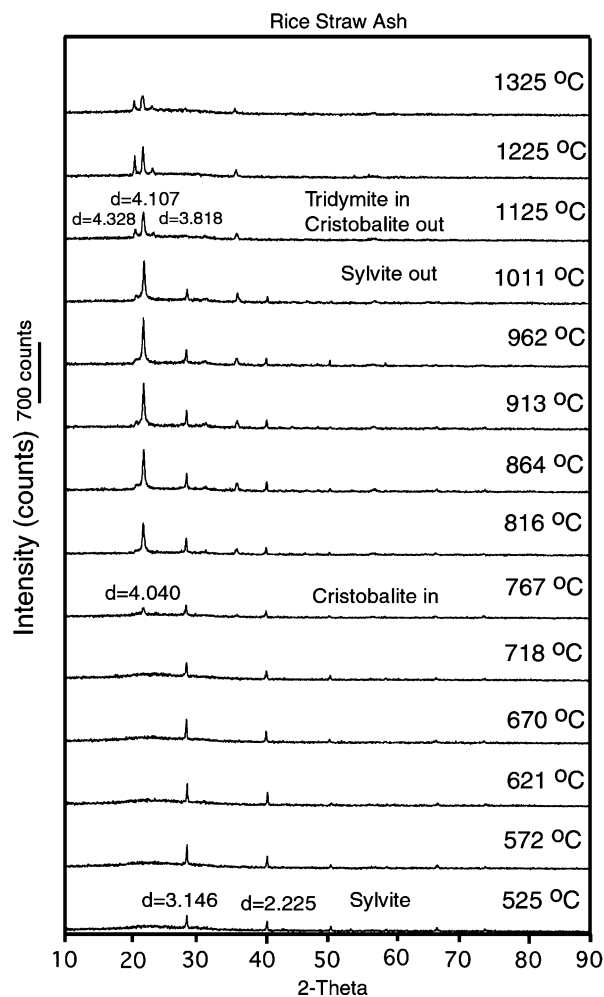


Fig. 8. Summary of XRD patterns (Cu K_α radiation) for the rice straw ashes. Characteristic measured *d*-values in ångstrom used to identify specific minerals.

tridymite is observed by the development of the 4.328 Å ($2\theta = 20.5^\circ$) and the 3.818 Å ($2\theta = 23.3^\circ$) diffraction peaks. The original 4.040 Å cristobalite diffraction peak shifts toward 4.107 Å at a 2θ of 21.6° . Additional silicate phases were not detected at or below the solidus. The weight loss does not show any clear correlation with the mineralogy.

The same rice straw ash was melted at high temperature by Thy et al. [10]. The melting behavior was interpreted to be strongly affected by loss of potassium. This resulted in a progressive rise in the liquidus and the coexistence of tridymite with liquid to temperatures well above the high- K_2O liquidus. Thy et al. [9] determined the liquidus temperature for a relatively similar rice straw ash at 1074 °C, again with tridymite on the liquidus.

Modeling using the FactSage thermochemical database [14] reproduced the essential features of the experiments. Melting is initiated between 600 and 700 °C and the liquidus is reached at 1500 °C, well above the experimental predictions. The dominant mineral predicted is a silica phase with the high-quartz to tridymite transition between 800 and 900 °C. This modeling result contrasts to the experiments that show a cristobalite to tridymite transition much higher at about 1125 °C. We speculate that this reversal in the expected appearance of the SiO_2 polymorphs may be due to the effect of release of K_2O from the ash. Potassium is in the model results released above 1000 °C mainly as KCl by the breakdown of sylvite.

The analytical results are summarized in Fig. 9 as K_2O normalized to the SiO_2 concentration (all wt%) and assuming that SiO_2 remains unchanged throughout the investigated temperature interval. The other oxides occur in low concentrations and record no detectable variation with temperature. The only compositional variation is a marked decrease in K_2O above 1225 °C.

The weight loss during firing shows systematic increase from 5.5% at 572 °C to 15% at 1225 °C (Fig. 5). The average weight loss determined in the melting experiments on the same ash by Thy et al. [10] was 15%. The loss-on-ignition at 950 °C is below 4% for all experiments fired above this temperature.

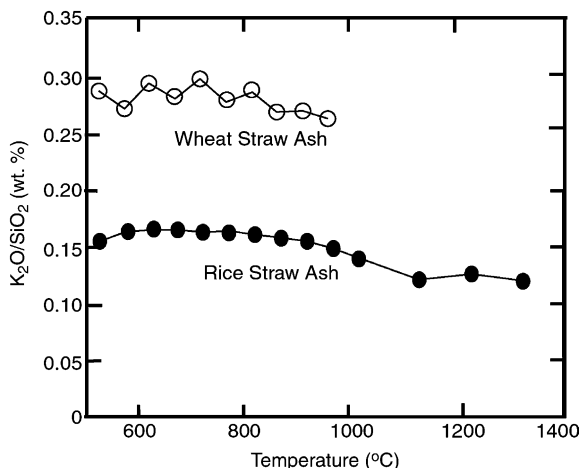


Fig. 9. K_2O content of the straw ashes normalized to SiO_2 content and plotted as a function of temperature.

The sum of the volatile losses suggests that most carbon and organic components were removed from the ash at temperatures above 1000 °C.

6.3. Wheat straw ash

The wheat straw ash was fired at temperatures from 572 to 962 °C, well into its melting interval. Significant hardening and sintering of the pellets occurs already from 572 °C. Large-scale melting is apparent at 816 °C with abundant bubble formation and pellet expansion. The ash color becomes systematically lighter with a yellowish tint from about 700–800 °C (L^* and b^* , Table 2).

The mineralogical changes as a function of temperature are similar to those observed for rice straw ash (Fig. 10). Sylvite is present throughout the investigated temperatures into the melting interval. Cristobalite appears at 718 °C. Tridymite does not appear probably because of the relatively low melting temperature or because of the relatively high potassium content. Additional phases were not detected despite that the experiments bracketed the solidus temperature.

Modeling using the FactSage database suggests very low initial melting temperature and a liquidus at 1300–1400 °C that

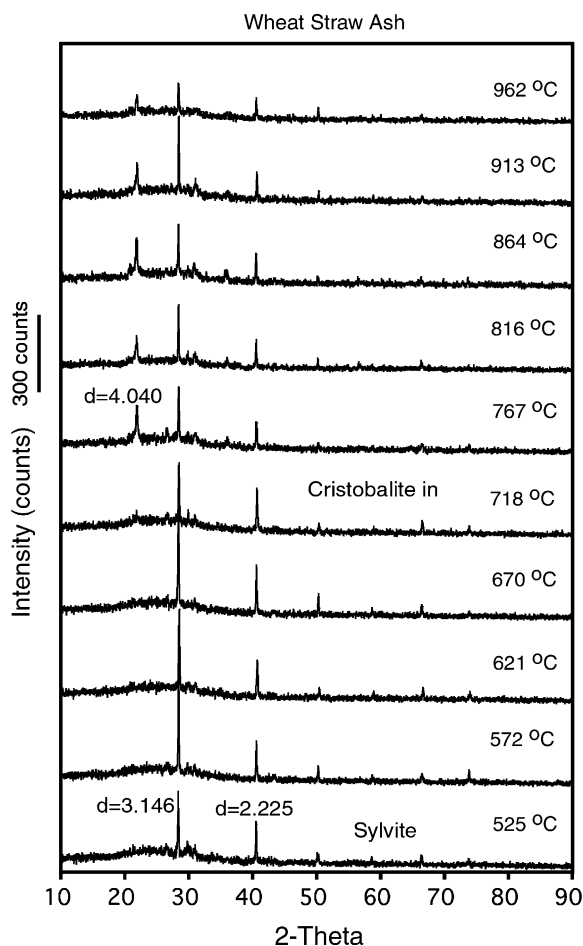


Fig. 10. Summary of XRD patterns ($Cu K_\alpha$ radiation) for the wheat straw ashes. Characteristic measured d -values in ångstrom used to identify specific minerals.

is unrealistically high compared to the experimental results. A high-quartz to tridymite transformation is modeled at 800–900 °C, although not observed in the experiments that contain cristobalite as the only stable SiO₂ polymorph. The modeling further suggests that the liquidus minerals are pyroxenes and that tridymite melts between 1100 and 1200 °C. As observed for rice straw, sylvite breaks down from 1000 °C to release potassium as KCl.

The analytical results are summarized in Fig. 9 as K₂O normalized to the SiO₂ concentration (all wt%) and assuming that SiO₂ remains unchanged throughout the investigated temperature interval. Similar to the rice straw ash results, most of the oxides occur in low concentrations that record no detectable variation with temperature. The normalized concentrations of K₂O vary significantly, but without any marked drop as for rice straw ash at high temperature.

Weight loss during firing (Fig. 5) shows systematic increase from 10.5% at 572 °C to 18.5% at 962 °C. The loss-on ignition determined at 950 °C reached a maximum of 7% and suggests that in part carbon or carbonates remained in the slag even in the 962 °C products. Localized carbon capture during melting of high silica biomass ash has previously been observed with rice hull [34].

6.4. Elemental losses during initial ashing

Because the K and Cl contents of the raw fuel are known (Table 2), expected concentrations in the ash can be calculated by comparing with the actual measured concentrations. Thus the loss of these elements during the initial ashing at 525 °C can be estimated.

The raw wood fuel contains 0.180 wt% K₂O. This recalculates into 16.7 wt% K₂O in ash or a loss of 26% during initial ashing. The raw rice straw fuel contains 2.40 wt% K₂O and 0.638 wt% Cl. This calculates as 11.7 wt% K₂O on an ash basis and does not suggest losses during initial ashing at 525 °C. Similarly, the Cl content of the raw rice straw fuel suggests a Cl content of 3.12 wt% on an ash basis, just below the measured concentration of 3.18 wt% Cl. The raw wheat straw fuel contains 1.43 wt% K₂O and 0.402 wt% Cl that recalculates into 15.8 wt% K₂O and 4.5 wt% Cl on an ash basis. Compared to the observed 16.6% this does not support significant loss of K₂O during initial ashing. However, similar comparison for Cl points toward a 20% loss of Cl during initial ashing.

6.5. Cl–K variation

Chlorine concentrations for the straw ashes show systematic variation with temperature (Fig. 11(a)). Until temperatures of about 770 °C, the concentrations steadily rise due to the removal of volatile components (Table 2). For temperatures above 770 °C, chlorine concentrations decrease, eventually leading to strong depletion in the rice straw ash. The wheat straw ash was not heated above 962 °C and, therefore, does not show the same strong depletion as does the rice straw ash, where temperatures of 1325 °C are reached with only 11% of

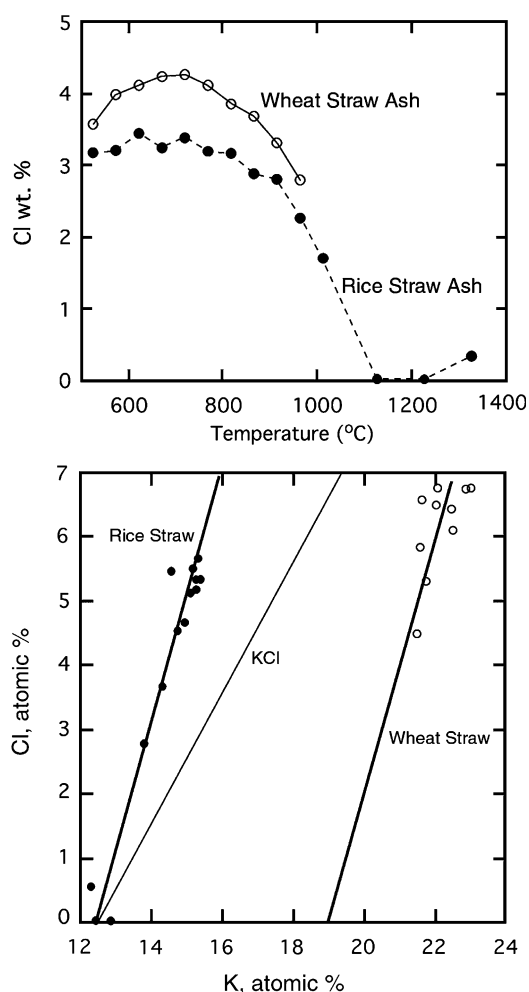


Fig. 11. Cl–K concentrations of straw ashes. (a) Cl content (wt%) as function of temperature (°C). (b) Cl concentrations (at.%) as function of K content (at.%). Linear correlation for rice straw ash is $Cl = -23.237 + 1.8675 \times K$ ($R^2 = 0.9711$).

the original chlorine remaining. This change in behavior is taken to reflect the breakdown of sylvite and the loss of Cl to the furnace atmosphere.

There is a strong co-variation between Cl and K calculated on an atomic basis (Fig. 11(b)). The rice straw ash with the strongest depletion in Cl shows a linear correlation between Cl and K ($\Sigma R^2 = 0.971$). The wheat straw ash shows a similar, but less-well defined variation. Extrapolation to Cl=0 suggests that a maximum of about 15% of K is lost to breakdown of sylvite (25% on a weight oxide basis). If the slope were controlled by breakdown of sylvite alone and the release of both K and Cl to the furnace atmosphere, the slope of the lines in Fig. 11(b) would have been 0.5 as opposed to the observed slopes of 1.8. This suggests that not all K released from breakdown of sylvite is lost from the ash and that 50% is retained.

7. Discussion

During combustion, the structure of plant material is decomposed and large volumes of organic components are released to the furnace vapor. Inorganic components either

form solid particles or are released as vapor species and transported to lower temperature regimes where reactions and deposition may occur. Organo-metallic complexes may also be volatilized prior to oxidation of the organic fraction. The experimental procedure used in this study was chosen to approach equilibrium conditions for the specific ash and temperature conditions. All experiments were conducted in air in an open system and used ashes produced at 525 °C as reactants. The procedure deviates from conditions experienced in operating boilers in not fully replicating the gas phase composition of the atmosphere surrounding the ash and heating at rates below those experienced when fuel particles are first injected into the furnace. The procedure also differs from other similar studies that often are conducted on raw fuels without an initial ashing stage [15,16]. The reason for the ashing pretreatment was the necessity of producing sufficiently large amounts (~10 g) of ash to allow high quality analysis of the composition of the experimental products. These experiments therefore are not intended to represent effects associated with short timescales prior to ash deposition or agglomeration.

For each fuel, a series of experiments were conducted at temperatures from the initial ashing conditions of 525 °C to within, if possible, the melting interval of the particular ash. Because the experiments were conducted on ashes, and not raw fuels, an evaluation of the elemental losses for critical elements (K, Cl) during the initial 525 °C ashing is relevant. The concentrations of K and Cl in the raw fuels were determined by a non-destructive technique (instrumental neutron activation). These analyses (Table 2) can be used to calculate the expected concentrations in the 525 °C ashes, since the moisture and ash content of the fuels are known. Comparison with the observed concentrations (Table 2), in general, suggests limited losses during the initial ashing for all type of fuels. Loss of K is either undetected or is relatively low for both straw fuels. A small loss of 26% K is suggested for the wood fuel; however, this is perhaps within the uncertainty considering the low ash content of wood. The Cl loss appears to be detectable during the initial ashing only for the wheat straw that has lost 25% of the Cl content of the raw fuel. It is of interest that there are no detectable losses for the rice ash during initial ashing, in contrast to the losses observed for wheat straw.

Studies of biomass pyrolysis have suggested losses up to 60% of Cl at relatively low temperatures (300–400 °C) [16–18]. Contrary to these results, the present study finds no significant losses at 525 °C for rice straw ash and only 25% loss of Cl for wheat straw ash. At higher temperature, approaching equilibrium melting of KCl at about 770 °C [19], the loss of Cl accelerates and rice straw ash reaches near complete depletion at 1125 °C (cf. [16,20]). Crystalline KCl persists in the straw ashes until temperatures of 962–1011 °C (Figs. 8 and 10), much higher than the expected breakdown of pure KCl at 770 °C and is present in partially melted wheat and rice straw ashes. This extended stability is likely caused by combinations of the failure to equilibrate the ash pellets to the experimental conditions and/or trapping of gas pockets in the pellets from which secondary condensation may occur during cooling.

The release of potassium is known to be dependent also on oxygen fugacity [20], but this effect is minimized in air.

Potassium shows losses positively correlated with temperature for all fuel ashes [20]. Most prominent is this for wood ash (Fig. 7) for which loss of potassium commences at about 1000 °C. The mineralogy of the products does not show the presence of potassium carbonate, despite detection by Misra et al. [15] and Olanders and Steenari [21] for coniferous wood/bark mixtures. Calcium carbonate is detected in the ashes to about 700–800 °C, after which calcite decomposes. Na–K carbonate may be stable at temperatures above 800 °C [14], but were not detected in this study. The retention of K₂O in the ashes to at least 1000 °C (Fig. 7), therefore, cannot be related to the presence of potassium carbonate or to the solubility of K in calcium carbonate. Other crystalline phases detected in the wood ashes are periclase and larnite (Fig. 7), which both contain little or no potassium. Detailed petrographic examinations of high temperature wood ash products by Thy et al. [10] revealed no other crystalline phases other than periclase and a phosphor-bearing larnite. It is possible that other wood fuel types may stabilize sulfates and silica [15,21], but such phases were not positively identified in this study.

Surprisingly, a third phase (with or without potassium) could not be detected at solidus and subsolidus conditions despite the multicomponent nature of wood ash (see also Ref. [10]). The release of potassium from the wood ash appears to be unrelated to the breakdown of potassium-bearing crystalline phases. Close inspection of the BSE and X-ray maps for the 525 °C wood ash suggests the presence of non-crystalline (or amorphous) grains. These are either small needle-shaped silica grains or larger, rounded to irregular shaped grains composed of Si and K or Ca and K. Dehydration and the breakdown of such amorphous grains and the formation of calcium silicates (larnite) are inferred to release potassium from the ash at temperatures above 1000 °C. High temperature melting experiments by Thy et al. [10] estimated by extrapolation an uncertain solidus between 1300–1400 °C. The study of Olanders and Steenari [21] of coniferous wood/bark mixtures detected Ca–Mg silicates (rankinite, merwinite, and larnite) and K–Ca silicates. The presence of quartz in many of their products suggests an ash composition with much higher activity of silica than in the very low silica wood ash investigated here (Table 1). Thy et al. [11] studied an urban wood fuel ash and reported Ca–Mg–Al silicates (melilite, garnet) and calcium phosphate, but did not report any potassium bearing silicates. Similarly, Thy et al. [10] identified Ca–Mg silicates (larnite, wollastonite, åkermanite, diopside) in mixtures of rice straw and wood ashes (same ashes as studies here). K–Al silicates (leucite) were only identified for mixtures with above 30% straw ash mixtures as a near solidus silicate that clearly affected the behavior of potassium. For the relatively clean wood fuel there is little support for stabilization of K or K–Ca silicates and thereby the retention of potassium in the ash or slag.

The straw ashes show more restricted potassium losses (8–20%) compared to wood ash (50%). The potassium content declines for both ashes from about 750 °C (Figs. 9 and 11).

The only mineral phase to stabilize in the straw ashes is cristobalite that appears at about 700–750 °C. Cristobalite is replaced by tridymite (both silica polymorphs) from about 1100 °C, probably due to the release of potassium and an associated change in bulk composition. No other silicate appears in the straw ashes as also confirmed by Thy et al. [10]. The only other mineral phase present is sylvite (KCl) that disappears above 1000 °C (Fig. 8), just before the replacement of cristobalite with tridymite. The Cl content declines from about 700 °C approximately when the potassium content also starts to decline. The release of potassium is possibly related to the breakdown of sylvite. The strong positive correlation between K and Cl shown in Fig. 11(b) indeed suggests that this is the case. However, about 50% of K (atomic basis) released from breakdown of sylvite is retained in the ash or slag in a solid or liquid form.

The solubility of Cl in potassium-bearing alumina-silicate melts is low (0.2–0.3 wt% Cl; [22,23]). The retention of chlorine in the ash is, therefore, best attributed to the presence of sylvite, as supported by the XRD results (Figs. 8 and 10). On the other hand, at high temperature, the concentrations of Cl in the rice straw ash converge toward levels that can be explained by the solubility in the silica-rich melt. Experimental studies of rice straw have shown that potassium is easily accommodated in the silicate melt formed at temperatures perhaps as low as 700–800 °C when binary K_2O – SiO_2 mixtures can be expected to start melting [24]. Hardening and sintering was observed from 572 °C in the present study, but no direct observation of the solidus was possible although an 800 °C solidus is generally accepted [25]. Thy et al. [10] melted the rice straw ash to 1536 °C and observed a positive correlation between K_2O loss and temperature. This loss persists for ashes without sylvite and points to the importance of release of potassium from the melt. Thy et al. [10] suggested that potassium is accommodated in the relatively open structure of highly polymerized straw ash melts. The distribution of potassium between melt and vapor was estimated at 0.4–1.0 (K_2O^{melt}/K_2O^{vapor}) for an urban wood fuel ash [11].

Direct measurements of the vapor release during combustion of straw material have been made by mass spectrometry [7,26]. The results by French and Milne [27] and Dayton et al. [28,29] using molecular beam mass spectrometry has concluded that potassium and chlorine are released to the vapor in molecular form (HCl, KOH, KCl). Thermodynamic modeling by Dayton et al. [29], Blander and Pelton [30], Jensen et al. [16], and Andersen et al. [31] has in general supported these measurements, but also suggested that metallic K may be released at temperatures above 1100 °C, consistent with the behavior of lunar material affected by high temperature impact processes [32,33].

8. Conclusions

The results of experimental heating of common biomass ashes (rice straw, wheat straw, and wood) from an initial ashing temperature of 525 °C to within their respective melting ranges are used to evaluate the behavior of volatile elements. Analyses

of major and minor element concentrations in the products reveal that only CO_2 , K_2O and Cl are lost in significant amounts from the ashes. The strongest loss of K_2O is seen for wood ash that has lost about 50% at 1425 °C, probably just above the solidus conditions. Chlorine is below the detection limit for the wood ash products. The rice straw ash shows much more restricted K_2O loss with about 20% lost at 1325 °C, well within the melting interval. The wheat straw ash melts at much lower temperatures and is nearly completely melted at 962 °C at which about 8% of K_2O is lost. Chlorine is positively correlated with potassium for both straw ashes. Sylvite (KCl) is present in straw ashes at least to 1010 °C, but chlorine concentration starts to decline already by 700–800 °C, consistent with the decomposition of sylvite. The release of chlorine thus appears to be attributable to the breakdown of crystalline KCl. There are no detectable silicate or carbonate minerals in the ashes that could accommodate potassium and whose breakdown could have explained the high temperature loss of potassium. Potassium only appears in crystalline form as KCl. The strong positive correlation between chlorine and potassium suggests that the breakdown of sylvite may in part control the release of potassium. About 50% of the potassium released from breakdown of sylvite was, however, retained in the ash or slag. Potassium losses persist well beyond the disappearance of sylvite in the straw ashes and are particularly strongly manifested in the wood ash that does not contain any potassium-bearing crystalline phases. It is suggested that the strong depletion seen in potassium at high temperature is caused by the dehydration, recrystallization, and partial melting of amorphous silicates. Potassium is either released to the vapor during melting or accommodated in the melt, approximately evenly distributed between melt and vapor. Potassium is partitioned into the vapor and melt because silicate minerals stabilized at high temperature, near or above the solidus, are devoid of potassium for both straw and wood ashes. At lower temperatures, well below the solidus, the breakdown of crystalline KCl may play a role in the release of potassium. The partitioning of chlorine into the vapor is much stronger than that for potassium by at least a factor of 2.

Acknowledgements

We acknowledge the help of John Neil and the access to the X-ray diffraction laboratory and the FactSage program package at the NEAT-ORU, Thermochemistry Facility, UC Davis. The University of California Energy Institute supported this study.

References

- [1] Marschner H. Mineral nutrition of higher plants. London: Harcourt Brace Jovanovich; 1986.
- [2] Miles TR, Miles Jr TR, Bryers RW, Baxter LL, Jenkins BM, Oden LL. Alkalis in alternative biofuels. FACT 18, Combustion modeling, scaling, and air toxins. New York: ASME; 1994 p. 211–220.
- [3] Jenkins, BM, Baxter, LL, Miles, TR, Miles, TR, Jr, Oden, LL, Bryers, RW, Winther, E. Composition of ash deposits in biomass fueled boilers: results of full-scale experiments and laboratory simulations. Kansas City, Kansas: ASAE International Summer Meeting, 1994.

- [4] Raask E. Mineral impurities in coal combustion. Washington, DC: Hemisphere Publishing; 1985.
- [5] Baxter LL. Biomass Bioenergy 1993;4:85–102.
- [6] Miles RR, Miles Jr TR, Baxter LL, Bryers RW, Jenkins BM, Oden LL. Biomass Bioenergy 1996;10:125–38.
- [7] Hastie JW, Plante ER, Bonnell DW. Alkali transport in coal conversion and combustion systems. In: Gole JL, Stwalley WC, editors. Metal Bonding and Interactions in High Temperature Systems With Emphasis on Alkali Metals. American Chemical Society Symposium Series 179; 1982, 1982. p. 543–600.
- [8] Jenkins, BM, Sime, M, Bakker, RR, Williams, RB, Baxter, LL, Turn, SQ, Thy, P, Leshner, C, Sclippa, G, Kinoshita, C. Combustion characteristics of high alkali biomass. Final report, Hawaii Natural Energy Institute. 1996.
- [9] Thy P, Leshner CE, Jenkins BM. Fuel 2000;79:693–700.
- [10] Thy, P, Jenkins, BM, Leshner, CE, Grundvig, S. Slag formation and potassium volatilization from rice straw blended wood fuel. Fuel Process Technol, in press.
- [11] Thy P, Jenkins BM, Leshner CE. Energy Fuel 1999;13:839–50.
- [12] Govindaraju, K. Geostandards Newsletter 1994; 18 (Special issue).
- [13] Govindaraju, K. Geostandards Newsletter 1995; 19 (Special issue).
- [14] Bale CW, Chartrand P, Degterow SA, Eriksson G, Hack K, Ben Mahfoud R, et al. Calphad 2002;26:189–228.
- [15] Misra MK, Ragland KW, Baker AJ. Biomass Bioenergy 1993;4:103–16.
- [16] Jensen PA, Frandsen FJ, Dam-Johansen K, Sander B. Energy Fuels 2000; 14:1280–5.
- [17] Björkman E, Strömberg B. Energy Fuels 1997;10:1026–32.
- [18] Olsson JG, Jaglid U, Pettersson JBC. Energy Fuel 1997;11:779–84.
- [19] Clark SP. J Chem Phys 1959;31:1526–31.
- [20] Enders M, Willenborg W, Albrecht J, Putnis A. Fuel Process Technol 2000;68:57–73.
- [21] Olanders B, Steenari B-M. Biomass Bioenergy 1995;8:105–15.
- [22] Carroll MR, Webster JD. Solubilities of sulfur, noble gases, nitrogen, chlorine, and fluorine in magmas. In: Carroll MR, Holloway JR, editors. Volatiles in Magmas. Reviews in Mineralogy, vol. 30. Washington D.C.: Mineralogical Society of America; 1994. p. 231–79.
- [23] Webster JD. J Petrol 1997;38:1793–807.
- [24] Kracek FC, Bowen NL, Morey GW. J Phys Chem 1937;41:1183–93.
- [25] Jenkins BM, Bakker RR, Wei JB. Biomass Bioenergy 1996;10:177–200.
- [26] Hastie, JW, Bonnell, DW, Plante, ER. Experimental and model determinations of coal mineral and slag phase-equilibria and alkali vapor-transport, VIII. In Bryers, RW and Vorres, KS, (eds.), Mineral Matter and Ash Deposition from Coal. Engineering Foundation Conference, Santa Barbara, CA., 1988.
- [27] French RJ, Milne TA. Biomass Bioenergy 1994;7:1–6.
- [28] Dayton DC, French RJ, Milne TA. Energy Fuel 1995;9:855–65.
- [29] Dayton DC, Jenkins BM, Turn SQ, Bakker RR, Williams RB, Belle-Qudry D, Hill LM. Energy Fuels 1999;13:860–70.
- [30] Blander M, Pelton AD. Biomass Bioenergy 1997;12:295–8.
- [31] Andersen KH, Frandsen FJ, Hansen PFB, Wieck-Hansen K, Rasmussen I, Overgaard P, Dam-Johansen K. Energy Fuel 2000;14:765–80.
- [32] Gibson EK, Hubbard NJ. Proc Third Lunar Sci Conf 1972;2:1367–80.
- [33] Maria GDe, Balducci G, Guido M, Piacente V. Proc Second Lunar Sci Conf 1971;2:1367–80.
- [34] Kaupp, A. Gasification of rice hulls: theory and praxis. Veiweg, 1984.